An Integrated Statistical, Geostatistical and Hydrogeological Approach for Assessing and Modelling Groundwater Salinity and Quality in Nile Delta Aquifer

Shaddad, Sameh; Castrignanò, Annamaria; Di Curzio, Diego; Rusi, Sergio; Salem, Hend S. Abu; Nosair, Ahmed M.

DOI
10.3390/agriengineering7020034

Publication date
2025

Document Version
Final published version

Published in
AgriEngineering

AgriEngineering

MDPI

Article

An Integrated Statistical, Geostatistical and Hydrogeological Approach for Assessing and Modelling Groundwater Salinity and Quality in Nile Delta Aquifer

Sameh Shaddad [1,*], Annamaria Castrignanò [2], Diego Di Curzio [3], Sergio Rusi [2], Hend S. Abu Salem [4] and Ahmed M. Nosair [5]

[1] Soil Science Department, Faculty of Agriculture, Zagazig University, Zagazig 44511, Egypt
[2] Department of Engineering and Geology (InGeo), Gabriele D'Annunzio University of Chieti-Pescara, 66100 Chieti, Italy; acastrignano53@gmail.com (A.C.); sergio.rusi@unich.it (S.R.)
[3] Department of Water Management, Delft University of Technology, 2628 CN Delft, The Netherlands; d.dicurzio@tudelft.nl
[4] Geology Department, Faculty of Science, Cairo University, Giza 12613, Egypt; hendsaeed@cu.edu.eg
[5] Environmental Geophysics Lab (ZEGL), Geology Department, Faculty of Science, Zagazig University, Zagazig 44511, Egypt; ahmed_nosair@zu.edu.eg
* Correspondence: smshaddad@agri.zu.edu.eg

Abstract: The phenomenon of seawater intrusion is becoming increasingly problematic, particularly in low-lying coastal regions and areas that rely heavily on aquifers for their freshwater supply. It is, therefore, vital to address the causes and consequences of this phenomenon in order to ensure the security of water resources and the sustainable use of water. The objective of this paper was twofold: firstly, to delineate zones with different salinization levels over time; secondly, to investigate the factors controlling seawater intrusion of the Nile Delta aquifer. Aquifer data were collected in Sharkia governorate, Egypt, over three historical periods of years: 1996, 2007, and 2018. The dataset used to create the linear model of coregionalization consisted of hydrogeological (water level), hydrodynamic (pH, EC, Na, Mg, K, Ca, HCO_3, SO_4), and auxiliary (distances from salt and freshwater sources) variables. Cokriging was applied to produce spatial thematic maps of the studied variables for the three years of the survey. In addition, factorial cokriging was applied to understand the processes beyond the change in the aquifer water quality and map the zones with similar characteristics. Results of mapping the first factor at long range over the three years indicated that there was an increase in seawater intrusion, especially in the northeastern part of the study area. The main cause of aquifer salinization over time was the depletion of the groundwater resource due to overexploitation.

Keywords: seawater intrusion; Nile Delta aquifer; multivariate geostatistics; groundwater salinity modeling

Academic Editor: Giovanni Rallo

Received: 6 December 2024
Revised: 19 January 2025
Accepted: 28 January 2025
Published: 31 January 2025

Citation: Shaddad, S.; Castrignanò, A.; Di Curzio, D.; Rusi, S.; Abu Salem, H.S.; Nosair, A.M. An Integrated Statistical, Geostatistical and Hydrogeological Approach for Assessing and Modelling Groundwater Salinity and Quality in Nile Delta Aquifer. *AgriEngineering* **2025**, *7*, 34. https://doi.org/10.3390/agriengineering7020034

1. Introduction

Coastal aquifers represent an important source of water, especially in arid and semi-arid regions. Stresses on coastal aquifers are related to salinization due to seawater intrusion (SWI) [1–5]. The main causes of SWI are the over-pumping of groundwater [6–8], sea level rise as a result of climate change and its subsequent global warming [9–12], and overpopulation along coastal areas [13–15]. Accordingly, SWI is seriously damaging the groundwater quality as well as soil, cultivation, and ecosystem [6,16–18]; therefore, the

management of SWI and the resulting environmental problems have become of research interest [19–21]. SWI in coastal areas has been assessed through different methodological approaches, such as hydrogeochemical investigations [7,22], geophysics [23,24], isotope hydrogeology [25,26], data analysis and numerical modeling [27–30], machine learning algorithms [31,32], and geostatistical modeling [33,34].

The majority of soils within the designated study area are classified as clay soils, which are characterized by their low hydraulic conductivity. These soils are particularly vulnerable to the deleterious effects of saline irrigation water, particularly when such water contains high concentrations of sodium and chloride ions. The presence of these ions has been shown to have a detrimental impact on the physical and chemical properties of soils, including alterations to soil structure and increased salinity [35]. The high sodium content of irrigation water reacts with soil particles, resulting in the exchange of sodium in the soil complex. This process leads to a dispersal effect, which, in turn, contributes to poor physical conditions in the soil. Additionally, the presence of chloride ions, in conjunction with sodium ions, contributes to elevated soil salinity, which has a detrimental effect on the water and nutrient uptake necessary for plant growth, given the increase in osmotic pressure of the soil solution. The repercussions of irrigating with saline water can be detrimental, potentially diminishing the potential yield of cultivated crops or constraining the range of cultivable crops. For instance, wheat yield exhibits a decline beginning at an irrigation water salinity of 4 dS/m and soil salinity of 6 dS/m [36].

The Nile Delta aquifer in Egypt is one of the most important aquifers in the world; however, it suffers from SWI in the coastal parts of the Mediterranean Sea as a result of anthropogenic impacts [7,37,38].

Due to the complexity of spatially and temporally variable processes that determine the salinity of subsurface aquifers, a reliable assessment of salinity-related risks is highly dependent on the ability of statistical tools to accurately capture spatial variability and to estimate the spatial relationships between salinity and other indicators of groundwater quality such as chloride and sodium content and electrical conductivity. The spatial association of the estimates of all these indicators at non-sampled locations with multivariate interpolation methods also makes it possible to delineate homogeneous areas by salinization level to be submitted to site-specific (differential) management. For these reasons, in this study, we used multivariate geostatistics as a branch of applied spatial statistics, which is based on a spatial dependence model to provide the prediction of indicators and the uncertainties of these predictions [39]. Above all, it is capable of combining different types of data with different physical and statistical properties, taking into account their proximity both over space and time and the different support of the measurements [40,41].

The objective of this paper was to delineate zones with different salinization levels over time and investigate the factors controlling seawater intrusion of the Nile Delta aquifer, using multivariate geostatistics compared with the classical analysis of the raw chemical data, with the perspective also to design effective groundwater management policies.

2. Materials and Methods

2.1. Site Location and Sampling Points

Figure 1 shows the location of the study area with the main freshwater/saltwater bodies and sampling points during the 1996, 2007, and 2018 surveys. The study area is surrounded by two freshwater bodies, i.e., Damietta branch and Ismailia Canal, and two saltwater bodies, which are the Suez Canal and Manzala Lake. The region's climate is typified by hot, arid summers and mild winters, with an annual precipitation level of 90–125 mm. The mean temperature in January and August in Zagazig, as measured over a 34-year

period from 1983 to 2016, was 13.0 and 29.3 °C, respectively. The relative humidity levels were recorded as 57% and 43% in January and August [42].

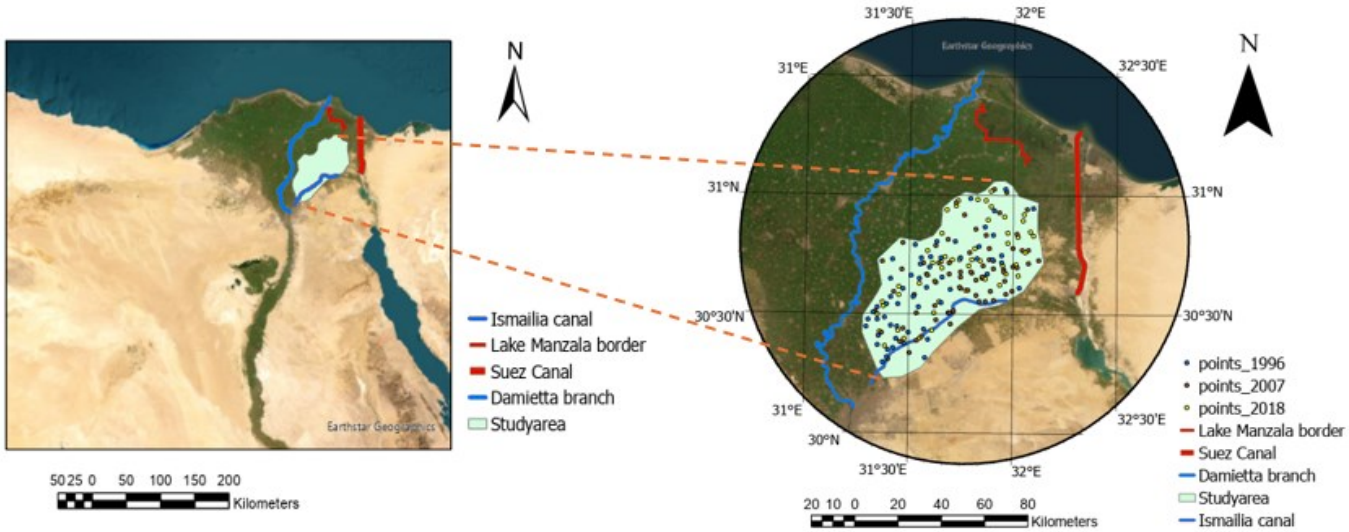

Figure 1. Locations of the study area with the main freshwater/saltwater bodies and sampling points during 1996, 2007, and 2018 surveys.

2.2. Hydrogeological Setting

The Nile Delta aquifer of Egypt is one of the most promising freshwater aquifers in the world. However, it suffers from saltwater intrusion from the north, where it is directly in contact with the Mediterranean coast. During the past 30 years, the aquifer has been severely pumped for domestic and irrigation purposes, which has been causing a direct impact on groundwater levels and its drawdown. This overexploitation of groundwater resources has caused significant salinization and successive well abandonment, especially in the central and northern parts of the Nile Delta.

The aquifer system is mainly represented by the sandy-gravelly Pleistocene aquifer with interbedded clay lenses (Mit Ghamr Formation) (Figure 2). This aquifer is overlaid by the upper Holocene sandy clay aquiclude layer (Bilqas Formation) and underlaid by the aquiclude Pliocene clays in some places and the Miocene limestone and marl in others [32,43](Figure 2a). The upper sandy clay cap layer is composed of Nile silty clay, silt, and sandy clay with varying thicknesses from about 20 m in the southern and central parts to about 70 m in the northern part [44]. The thickness of the Pleistocene aquifer increased towards the coastal area [7,45,46], where it usually varies between 250 (southern portion) and 900 m (northern portion). The Pleistocene aquifer varies between the unconfined conditions in the southeastern parts, from semi to unconfined conditions in most eastern and northern parts, and confined conditions in central and western parts of the study area. This variation in the aquifer nature is related to the lithological composition and/or missing of the upper Holocene cap cover, which serves in some areas as an aquitard layer of coarser grains, allowing upward leakage or downward flow [37,43]. The distributed freshwater canals (Figure 2b) on the River Nile, which dissect the Holocene cap layer, represent the main source for the aquifer recharge in addition to the contribution of irrigation return flow [37,47].

The hydrogeological setting summarized above, combined with the fact that all the wells analyzed are limited to a maximum depth of 130 m (with an average of 57 m), allows us to consider a study volume contained in a single multilayer aquifer mostly developed between Holocene sandy clays and Pleistocene clayey sands. This assumption is

corroborated by the presence of intervals of clayey sands within the Holocene succession and sandy clays within the Pleistocene succession. Groundwater levels in the Pleistocene aquifer decrease towards the northern parts and range from 8 to 14 m above sea level (m asl) in the southern parts of the Nile Delta to less than 1 m asl in the northern parts [43,44,46,48].

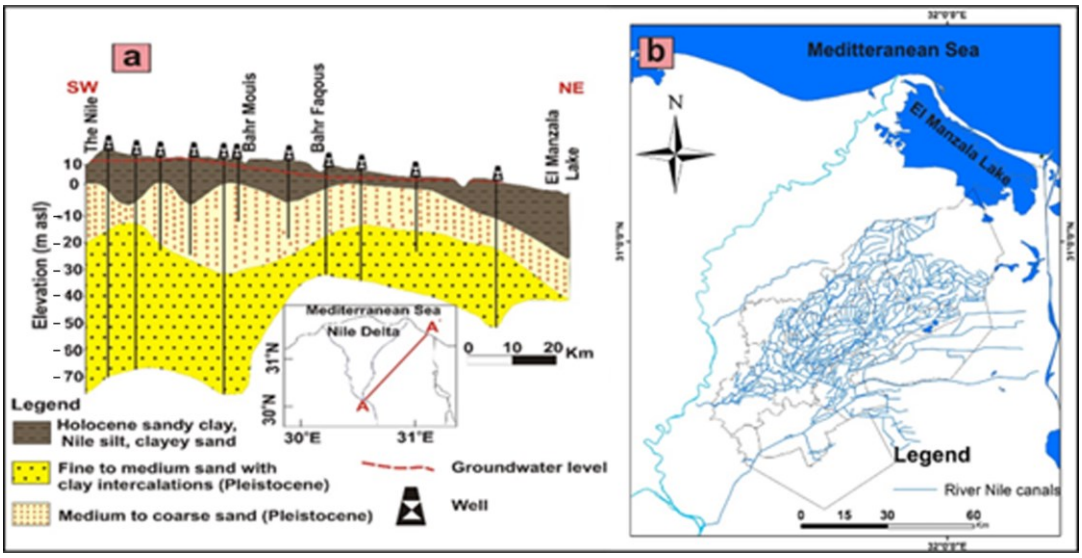

Figure 2. (**a**) Hydrogeologic cross section in the eastern Nile Delta aquifer [44]; (**b**) River Nile freshwater canals.

2.3. Data Collection

Hydrochemical and hydrogeological data of the Nile Delta aquifer in the study area of three sampling campaigns of years, 1996, 2007, and 2018, were used, which considered different monitoring networks (Table 1) and whose sampling points had variable total depths. The monitoring networks also included hand dug wells (18–45 m depth), irrigation wells (35–90 m wells), and drinking wells (100–120 m depth).

Table 1. Description of the sampling campaigns.

Year	Number of Points	Depth Range	Reference
1996	56	20–140 m	[48,49]
2007	67	10–120 m	[46]
2018	60	18–120 m	[32]

Before collecting groundwater samples (the year 2018), each well was purged for at least 30 min to remove stagnant water. Total dissolved solids (TDS), pH, and electrical conductivity (EC) were measured in the field prior to the sample collection by using calibrated field Orion portable meters (Thermo Scientific, Singapore). The collected samples were stored in iceboxes and sent to the central laboratories of the Productive Sufficiency Institute (PSI) at Zagazig University for different hydrochemical analyses. The data were used to construct a detailed database of the aquifer water quality over time.

Ion chromatography (Dionex ICS-1100) was used to analyze the major cations and anions (Mg^{2+}, K^{+}, Ca^{2+}, Na^{+}, SO_4^{2-}, and Cl^{-}), while HCO_3^{-} was determined by titration using H_2SO_4 (0.01 N).

2.4. Raw Chemical Data

In order to characterize the hydrogeochemical structure of the aquifer and to compare the geostatistical approach with the traditional one, geostatistical calculations were

supported by analysis techniques typical of hydrochemistry. For this purpose, the hydrochemical data set was processed, classified, and compared for each year of the survey using the Schoeller–Berkaloff graph.

The Schoeller Berkaloff graph can be used both to classify a single water sample and to classify and compare more than one sample. It consists of a graph with the main cations and anions dissolved in water (Ca, Mg, Na + K and Cl, SO_4, $HCO_3 + CO_3$) positioned on the horizontal axis and the concentrations of the ions, expressed in meq/l, on the logarithmic vertical axis. Each water sample will, therefore, be represented by a broken line joining the concentrations, which will highlight the presence of dominant, secondary, and minor ions. The analysis of two or more broken lines (groups of broken lines) will allow us to perform comparisons between the represented waters based on chemistry. In this type of graph, waters with the same concentration but different chemistry will then be easily distinguishable. The graph can also show the relationships between various ions in a water sample or a group of water samples. The raw water chemistry data were also analyzed with regard to their spatial distribution with various geospatial techniques to provide spatial distribution maps for each ion and each survey year, which will be discussed in Section 2.4. The analysis of the chemistry of the waters with the Schoeller Berkaloff graph allowed us to select the dominant ions of the waters, which, together with salinity (represented by Electrical Conductivity), were used in the creation of the spatial distribution maps. To verify any piezometric and groundwater flow variations, the maps of water levels over the three years were also estimated and compared with hydrochemical ones.

The evolution of water chemistry over time was analyzed with the Schoeller Berkaloff graphs and the Q-Q plots of water level, EC, Cl, Na, and Ca for the pairs of contiguous surveys 1996–2007 and 2007–2018. The Q-Q Plot graphs (which relate the quantiles of a physical or chemical property in two different surveys) were not created with raw data but from the geostatistical estimations due to the non-congruence of measurement locations among different surveys. The graphs compare two data distributions, and if there is no perfect consistency, the data depart from the bisector of the first quadrant.

2.5. Data Processing

Exploratory analysis was aimed at describing statistically the data distributions of the variables. Conventional basic statistics, including maximum, minimum, mean, median, standard deviation (SD), skewness, and kurtosis, were calculated.

A Q-Q plot was used to compare the data distribution of the same variable over time. Although the interpolation techniques of geostatistics are not parametric, in the case of strongly skewed distributions, to facilitate the variogram fitting process and produce an estimate of uncertainty [50], it was preferred to transform all variables characterized by measurement unit and magnitude different into standardized Gaussian variables with zero mean and unit standard deviation. For this purpose, Gaussian anamorphosis was performed by using an expansion of Hermite polynomials truncated at the first 100 terms [40,51].

Multivariate Geostatistical Analysis

For a detailed description of the multivariate techniques of geostatistics, references are made to the many textbooks on the subject [39,51, 52]. Only those techniques most closely specific to the case study will be briefly mentioned here. For each survey date (1996, 2007, and 2018), a coregionalization dataset was created as follows: at each well location, together with the hydrochemical sample data, three auxiliary raster variables were collocated by migration of the pixel to the nearest sampling point. The auxiliary variables were the minimum distance from the Damietta branch, which is a branch of the Nile River located in the west-northern part of the study area as an indicator of freshwater

resources; the distance from the Manzala lake located in the northeastern part of the study area and the Suez Canal, located in the eastern part of the study area, as an indicator of saltwater resource (Table 2). The distances of the three auxiliary variables were calculated using the Near tool, which is available in the ArcGIS Pro 2.7.0 software developed by ESRI. The tool calculates the distance and additional proximity information between the input features and the closest features in another layer or feature class using the tools available in ArcGIS Pro 2.7.0, USA.

Table 2. Point sample variables and auxiliary variables were used to create the LMC in the three sampling dates.

Year	Number of Point Samples	Point Sample Variables	Number of Auxiliary Variables Points Based on 1000 m × 1000 m Grid	Auxiliary Variables
1996	56	Water level, pH, EC, Na, K, Ca, Mg, Cl, HCO_3, SO_4	4322	Minimum distances from Damietta branch, lake Manzala and Suez Canal
2007	67	Water level, pH, EC, Na, K, Ca, Mg, Cl, HCO_3, SO_4	4322	Minimum distances from Damietta branch, lake Manzala and Suez Canal
2018	60	Water level, pH, EC, Na, K, Ca, Mg, Cl, HCO_3, SO_4	4322	Minimum distances from Damietta branch, lake Manzala and Suez Canal

The whole set of both experimental direct and cross-variograms was fitted to a Linear Model of Coregionalization (LMC) [53], which considers all the studied variables as the result of the same independent physical processes acting over different spatial scales. All direct and cross semi-variograms of the variables are then modeled as a linear combination of standardized semi-variograms of the unit sill, each one corresponding to an identified spatial scale.

The sills of the direct and cross variograms of each scale constitute a matrix called coregionalization matrix, which must be a symmetric positive semi-definite matrix. Each coregionalization matrix can be interpreted as a variance-covariance matrix specific to a given spatial scale [54].

Multi-Collocated Cokriging

Ordinary cokriging (OCK) is one of the most basic multivariate geostatistical methods of interpolation, where the local mean is assumed to be constant but of unknown value. A way of integrating secondary finer resolution grid information into primary sparse variable modeling is multi-collocated cokriging [55]. It is a technique that is very similar to ordinary cokriging, but the only difference is the neighborhood search. Since using all the secondary exhaustive information contained in the neighborhood can lead to an intractable solution due to too much information, the secondary variable is used only at the target location and also at all locations where the primary variable is defined. It is less accurate than full cokriging because it does not use all the auxiliary information contained within the neighborhood, but it is much less computationally intensive. Nevertheless, as the colocated secondary datum tends to screen out the influence of more distant secondary data, there is actually little loss of information.

Cross-validation

This involves deleting each sample in turn and then kriging it (z^*) independently of all other points in the estimation neighborhood [56].

Two statistics [55], defined as follows, were used to evaluate the performance of the LMC using cross-validation:

$$ME = \frac{1}{N}\sum_{i=1}^{N}(z_i - z^*)$$

$$MSSE = \frac{1}{N}\sum_{i=1}^{N}\left(\frac{z_i - z_i^*}{\sigma_i}\right)^2$$

where N is the number of active observations and σ_i the cokriging standard deviation of the estimate z_i^*.

For an unbiased and accurate estimate, ME should be near 0 and MSSE near 1 because the latter approximately represents the ratio of an experimental and a theoretical variance [57]. However, if MSSE is different from 1 but within the tolerance interval $(1 - 3\sqrt{\frac{2}{N}};\ 1 + 3\sqrt{\frac{2}{N}},)$ [51], the estimation may be considered accurate.

Factor cokriging analysis (FCA)

To synthesize the complex multivariate variation of the study area in a limited number of roughly homogeneous macro-zones, which could, therefore, be subjected to differential management, factor cokriging analysis (FCA) was applied using the same LMCs previously estimated for each sampling date.

FCA is quite similar to the traditional Principal Component Analysis (PCA) but with the difference that each coregionalization matrix (corresponding to a given spatial scale) is broken down into the eigenvalues and eigenvector matrices [52,58,59]. In FCA, only the eigenvectors, called regionalized factors (FC), corresponding to eigenvalues greater than one, were retained because they describe a larger portion of the spatial variance than that of each variable standardized to variance 1. The regionalized factors corresponding to the nugget effect were omitted, as they are mostly affected by measurement errors.

Mapping the estimated retained regionalized factors provides a synthetic illustration of the behavior and relationships among variables at different spatial scales. The interpolation of the FCs is performed by solving a modified cokriging system, as described by[60].

3. Results

3.1. Exploratory Data Analysis

Table 3 shows the descriptive statistics of the whole dataset for the three different surveys. This has been performed to investigate the shape of the data distributions before carrying out the geostatistical analysis. The skewness values reported in Table 3 indicate that most of the study variables for each survey are skewed either positively or negatively except for total depth in 1996 and 2007 and water level in 2018. Therefore, all variables were transformed using the Gaussian anamorphosis prior to geostatistical analysis.

Table 3. Descriptive statistics of studied parameters in 1996, 2007, and 2018.

Statistic	Sampling Year	Total Depth (m)	Water Level (m)	pH	EC dSm^{-1}	Ion Concentration in mg/l						
						K	Na	Mg	Ca	Cl	SO_4	HCO_3
Mean	1996	76.5	6.85	8.4	2.78	11	377	78	131	643	362	267
STD		32.2	2.62	0.6	5.26	17	721	167	287	1675	1017	175
Variance		1039.6	6.88	0.4	27.66	299	519,669	27,985	82,401	2,805,187	1,033,345	30,593
Kurtosis		−0.6	−1.53	4.5	14.84	15	13	15	17	18	32	6.6
Skewness		−0.17	0.02	−1.8	3.82	3.7	3.6	3.9	4	4.2	5.4	2.3
Minimum		20	1.8	6.3	0.34	1	27	8	10	18	10	19
Maximum		140	10.75	9.7	26.75	90	3620	850	1623	9500	6900	1006

Count		56	56	56	56	56	56	56	56	56	56	56
Mean		50.2	5.53	7.5	2.38	8	325	45	113	461	202	295
STD		23.9	1.78	0.3	3.70	6	460	91	166	1118	207	85
Variance		572.4	3.16	0.09	13.69	42	211,539	8331	27,707	1,250,968	42,795	7311
Kurtosis	2007	−1.17	0.00	1.1	20.92	10.7	16	24	21	24	3	0.01
Skewness		0.15	0.80	1	4.51	3	3.8	4.9	4.4	4.9	1.8	−0.41
Minimum		15	2.5	7.0	0.40	1.7	28	3.6	12	17.8	10	65
Maximum		105	10	8.5	20.73	39	2560	545	1020	6560	887	480
Count		67	67	67	67	67	67	67	67	67	67	67
Mean		48.7	4.11	7.57	5.43	24	734	146	227	1459	654	227
STD		31.2	1.45	0.38	8.14	26	1131	242	366	2556	1147	129
Variance		975.4	2.12	0.15	66.18	702	1,279,571	58,457	134,023	6,535,520	1,315,862	16,709
Kurtosis	2018	−0.02	−0.52	3.08	2.35	8.8	2.3	3.8	4	3.7	4.3	5.8
Skewness		1.12	−0.02	1.55	1.94	2.8	1.9	2.2	2.2	2.2	2.3	1.9
Minimum		18	0.75	6.9	0.389	4.5	16	13	15	30	15	72
Maximum		120	6.7	8.9	30.03	146	4350	960	1554	10,120	4560	810
Count		60	60	60	60	60	60	60	60	60	60	60

3.2. Raw Hydrochemical Data

The chemical analyses of all samples for each survey, processed through the Schoeller–Berkaloff diagrams (Figure S1), show the presence of two main groups of water: predominantly calcium and/or sodium bicarbonate (Figure S1B,E,H) and predominantly sodium chloride (Figure S1C,F,I). The first group includes waters with chemical formula:

Na, Ca, Mg–HCO_3, Cl, SO_4; Ca, Na, Mg–HCO_3, Cl, SO_4; Mg, Ca, Na–HCO_3, Cl, SO_4.

The second group includes waters with chemical formula:

Na, Ca, Mg–Cl, SO_4, HCO_3; Na, Mg, Ca–Cl, SO_4, HCO_3; Na, Ca, Mg–Cl, HCO_3, SO_4.

The cations of the first group (bicarbonate–calcium/sodium waters) do not show the prevalence of a particular ion, but moving from the first to the last sampling campaign, they show a decrease in the samples with high Na and K contents. Regarding anions, the HCO_3 content remains constant over time, while variability in the Cl and SO_4 contents is observed. Concentrations are between 1 and 10 meq/l.

In the second group (sodium chloride waters), the concentrations are higher and vary from 1 to over 100 meq/l and, therefore, more than 10 times the concentrations of the first group. This situation is clearly visible in the Scholler Berkaloff diagrams, which show the water types of the second group located in the upper part of the graph. The concentrations also show a slight increase in values over time and a high variation in SO_4 content, so much as to highlight the presence of some sulfate–alkaline samples.

3.3. Geostatistical Results

Linear model of Coregionalization

Three linear models of coregionalization of the transformed Gaussian variables were applied for three periods: 1996, 2007, and 2018 (Tables S1, S2, and S3, respectively)

Since it was not possible to check whether any anisotropy existed given the small number of samples, it was preferred to fit an isotropic model of spatial dependence. LMC developed for the dataset collected in 1996 involves three spatial structures: a nugget effect, a spherical model with a range of 1200 m, and a Bessel-K model with a range of 100,000 m; the one from 2007 involves three spatial structures: a nugget effect; a spherical model with a range of 10,000 m and a Bessel-K scale with a range of 100,000 m (Table 4); the one from 2018 involves three spatial structures: a nugget effect; a spherical model with a range of 1000 m and an isotropic Bessel-K scale with a range of 100,000 m.

Table 4. Linear Model of Coregionalization of the variable sets is shown in Table 2. For each year, a nugget effect was included.

Year	Structures	Range
1996	Spherical	1200 m
	k-Bessel	100,000 m
2007	Spherical	10000 m
	k-Bessel	100,000 m
2018	Spherical	1000 m
	k-Bessel	100,000 m

As can be seen, the spatial structures, apart from absolute values of the parameters, remain invariant enough over time, especially those related to the long-range, most likely associated with hydrogeological characteristics that do not change over time. On the contrary, it is different for the shorter-range structure, which has a variable range over time because it is more related to anthropogenic activity and possible movements of groundwater flows (saline water intrusion and/or freshwater adductions).

3.4. Spatial Distribution

The multi-collocated cokriging based on the LMC allowed for estimating the spatial distribution of water levels (Figure 3), EC, Cl, Na, and Ca. Pumping-induced water level variation is usually considered the main anthropogenic cause of SWI, whereas the four physicochemical variables can be considered as hydrogeochemical proxies of aquifer salinization, as they describe the increase in groundwater salinity and water type [61].

In Figure 4, the water level evolution is reported from which it is possible to note the following:

- In 1996, a regular piezometric distribution with almost homogeneous gradients and flow lines perpendicular to the coastline and parallel to the Damietta Branch of the Nile was established.
- In 2007, less regular distribution of the piezometric surface was observed, with a lowering of the water level in the central and southern parts and the presence of concentrated recall zones in the central part.
- In 2018, a further generalized reduction in water level was observed in the southern and northern portions of the study area, and there was a greater number of water recall areas than in 2007. In the central part, however, a recovery in the water level was observed, which gave rise to a lobed shape of the piezometric surface (encircled in red in Figure 3), which indicates an alternation of areas of probable attenuation of the pumping.

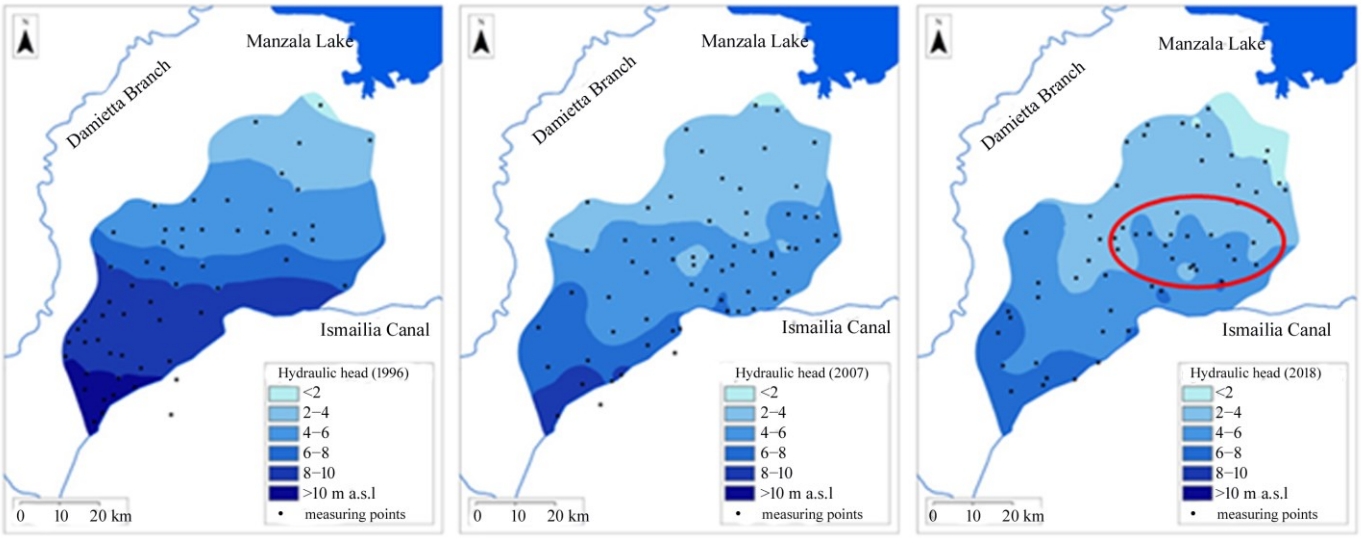

Figure 3. Cokriged maps of water level during the three surveys (1996, 2007, 2018). In 2018, the red ellipse encircles a lobed shape piezometric surface that indicates a recovery in the water level.

The thematic maps of groundwater salinity (expressed in EC) are shown in Figure 4, where a clear trend of increasing salinity towards the coastal area can be seen in the 1996 survey. In the 2007 survey, the level of salinization increased even further, especially nearer the Manzala Lake. The pattern of salinity in the 2018 survey is somewhat similar to that of 2007, with salinity increasing towards the northwest part of the study area. It is worth noting that in the 2018 survey, two zones of groundwater salinity less than 2 dS/m appeared in the eastern part of the study area, corresponding to the lobate shape of the piezometric surface described above.

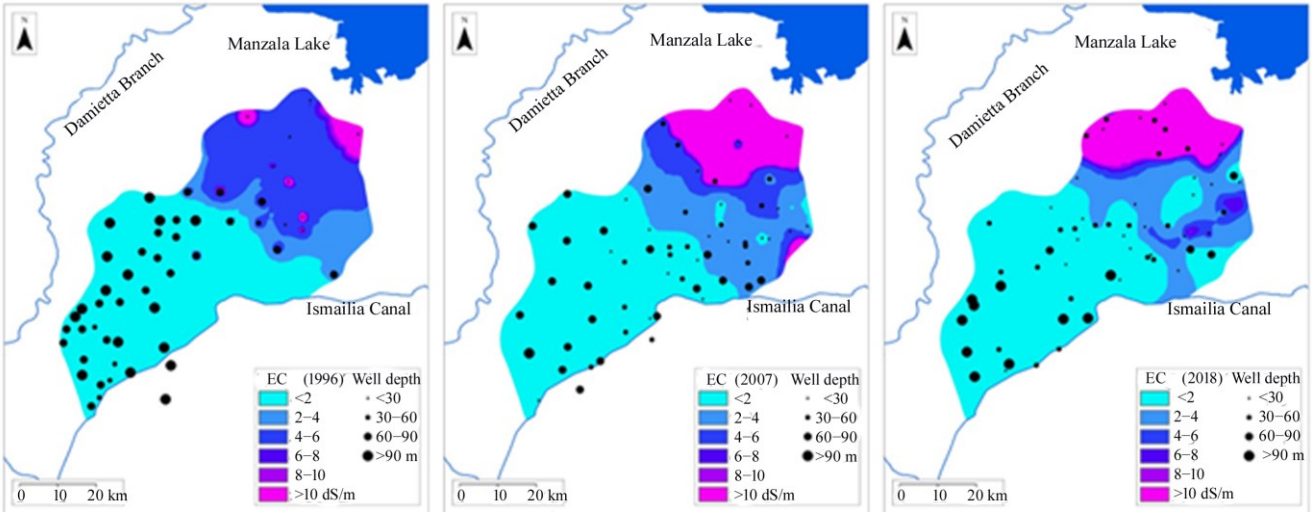

Figure 4. Cokriged maps of EC during the three surveys (1996, 2007, 2018).

The spatial distribution of chloride (Figure 5) during the reference years was consistent with the EC one. The lower concentrations of chloride in the southwestern part might be attributed to the proximity of freshwater sources, such as the Damietta branch and the Ismailia canal. It is worth noting that in 2007, chloride concentrations in the northern part increased dramatically from around 1000 mg/l to more than 1500 mg/l, compared to the chloride concentrations on the 1996 map. This evidence likely relates to groundwater overexploitation for crop irrigation in this cultivated area. This interpretation is further supported by the decrease in water level between 1996 and 2007 (Figure 3).

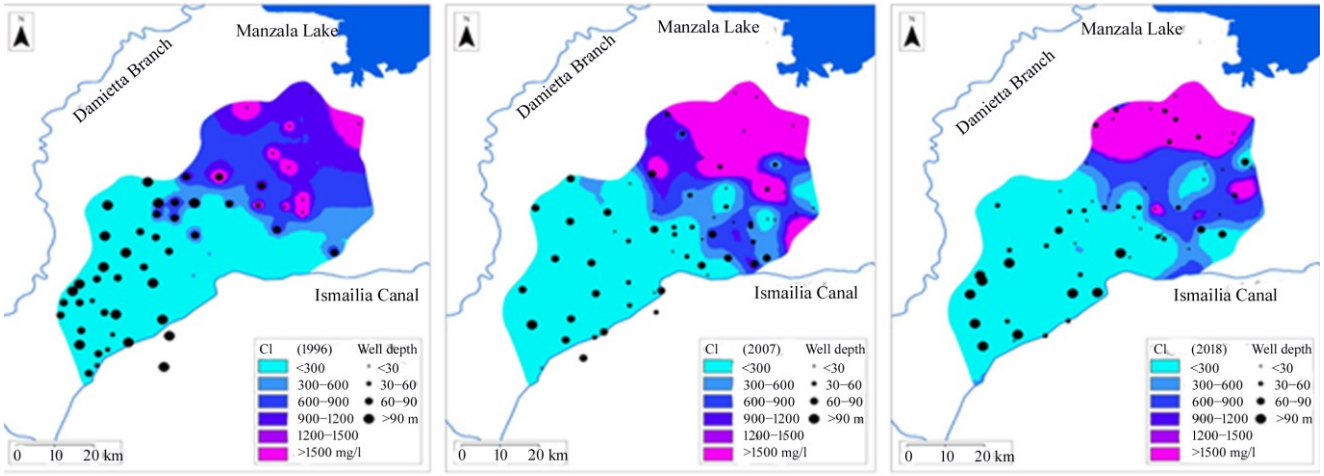

Figure 5. Cokriged maps of chloride during the three surveys (1996, 2007, 2018).

The sodium spatial distributions (Figure 6) show that in 2007, sodium concentrations increased from the northern part towards the southwestern part, covering about 40% of the study area and reducing the water quality of the wells.

For both chlorides and sodium in 2018, there was a slight decrease in the areas with the highest concentrations. Furthermore, the spatial distribution shows some zones located in the northeastern part with lower sodium concentrations of less than 100 mg/l, once again at the lobate piezometric surface.

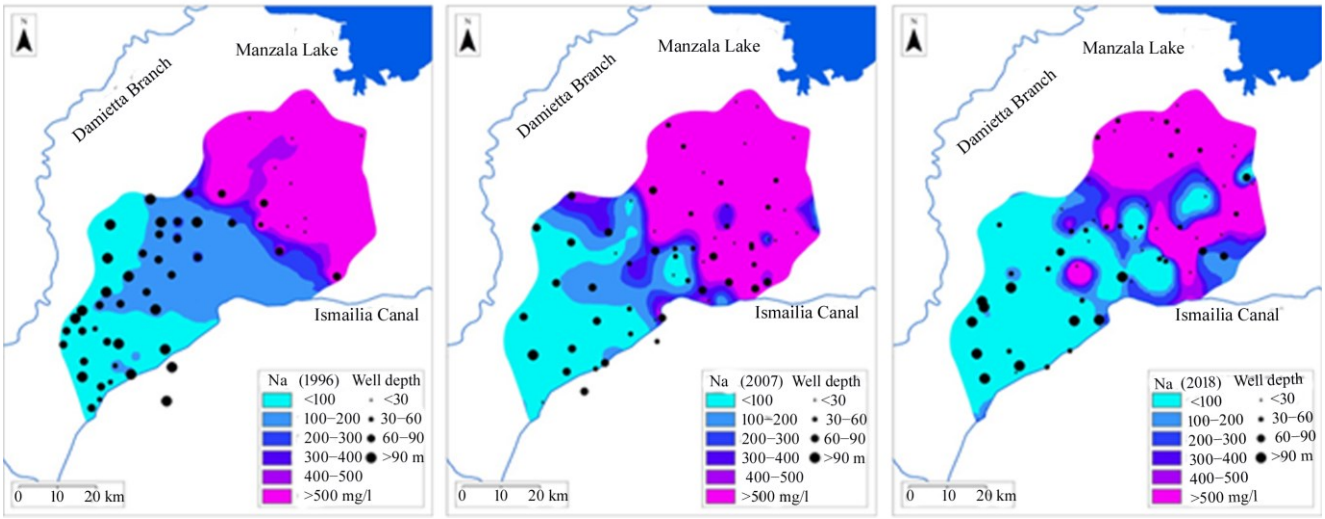

Figure 6. Cokriged maps of sodium during the three surveys (1996, 2007, 2018).

Figure 7 shows the spatial maps of calcium, where an opposite pattern to that of EC, Cl, and Na was observed. Its concentration decreased, especially in the northern part, in 2007. Comparing the calcium concentrations between 2007 and 2018, an increase in calcium concentrations can be seen in the northeastern part. New zones of high calcium concentrations appeared in the central part of the 2018 map, corresponding to the lobed zone of the piezometric surface.

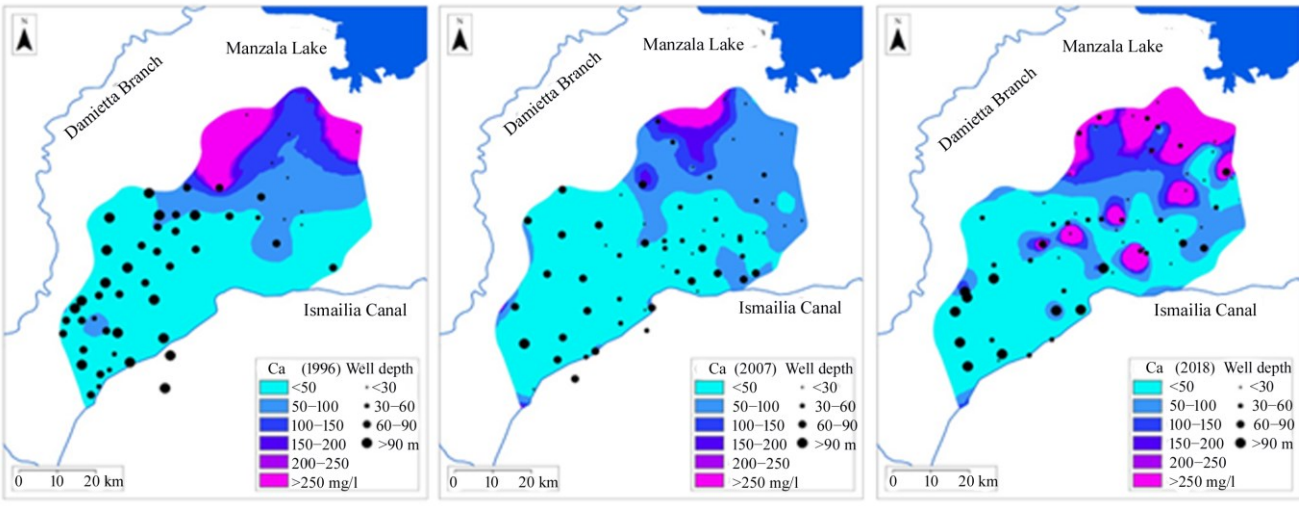

Figure 7. Cokriged maps of calcium during the three surveys (1996, 2007, 2018).

Considering the spatial distribution obtained from the Cokriged maps described above and to better describe the evolution of chemistry over time, the Q-Q plot graphs (Figures 8 and 9) describing the evolution of the estimated EC, Cl, Na, and Ca are shown below in relation to the water level.

Moreover, to analyze the evolution of SWI at a regional scale and over the considered period, we took advantage of Q-Q plots to compare the estimated proxy variables (i.e., water level, EC, Cl, Na, and Ca) and interpret the results from a hydrogeological and hydrogeochemical standpoint (Figure 8).

As for the estimated water levels between 2 and 4 m a.s.l., no significant changes were observed between 1996 and 2007. However, for values between 4 and 10 m a.s.l., there was a significant decrease in 2007 compared to 1996, indicating a decrease in the water level.

In the second period, from 2007 to 2018 (Figure 9), the water levels decreased but in a less evident way. This probably means a decrease in pumping rates compared to the previous period.

For groundwater salinity, the estimates for up to 5 dS/m remained almost the same for both the years 1996 and 2007 (Figure 8). However, there was an increase in water salinity, especially for the estimates between 5 and 25 dS/m in 2007, indicating that the water salinity level increased during the period 1996–2007. When comparing 2007 and 2018, no significant changes were observed. The only change was the increase in salinity for values above 23 dS/m in 2018. A similar trend to that observed for salinity was observed for chloride, which shows that it increased between 1996 and 2007 (Figure 8), whereas it remained slightly higher in 2007 than in 2018 up to the value of 8000 mg/L, beyond which the trend reversed.

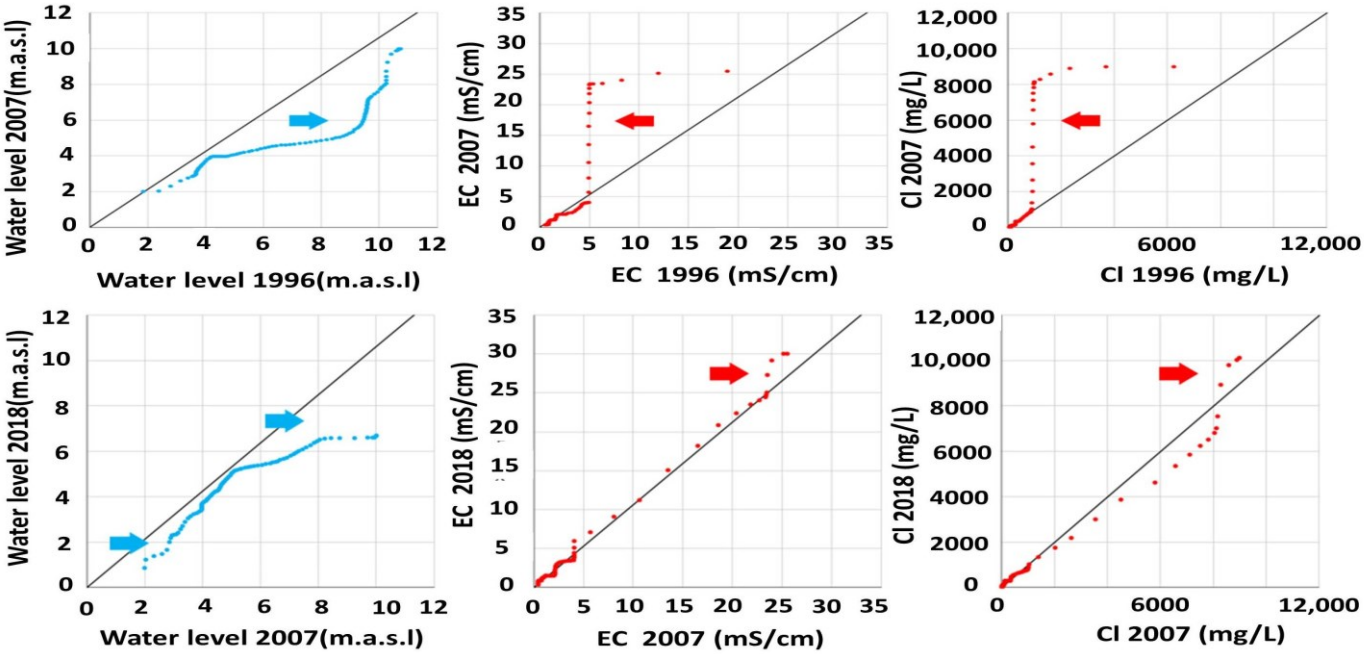

Figure 8. Q-Q plots for water level, EC, and Cl (1996 vs. 2007 and 2007 vs. 2018).

There was an increase in sodium concentration in 2007 compared to 1996 (Figure 9), whereas an opposite pattern was observed in 2018 compared to 2007, indicating a decreasing Na concentration during the period 2007–2018, quite similar to the behavior of Cl. Regarding the calcium content, the Q-Q plot (Figure 9) of 1996 vs. 2007 shows that there was a decrease in its concentration in 2007 compared to 1996, especially for the values of 120 mg/L and above. Differently, calcium concentration increased in 2018 compared to 2007.

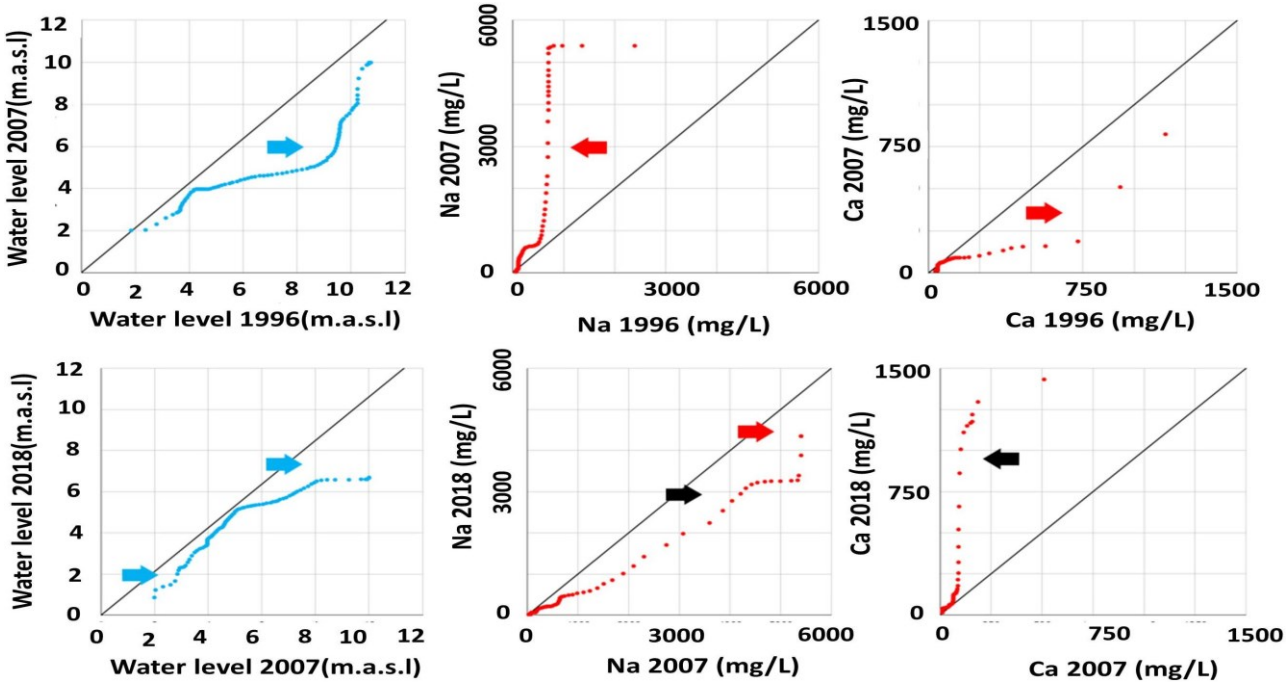

Figure 9. Q-Q plots for sodium and calcium (1996 vs. 2007 and 2007 vs. 2018).

Ultimately, the Q-Q plot graphs graphically render what is already evident in the analysis of the spatial distributions in the three study periods. However, it is a concise

though non-spatial way of characterizing the entire distribution of waters at the three survey dates.

Delineation of homogenous zones based on factorial kriging

Tables S4–S6 show the structure of the regionalized factors whose eigenvalue is greater than 1 by spatial scale and survey. In 1996 (Table S4), on the first long-range factor with an eigenvalue greater than 1, which explained 46.56% of the spatial variance at that scale (100,000 m), the distance from the freshwater source (Damietta branch), EC and Cl weigh more and positively, whereas the distances from the saltwater sources (distance from Lake Manzala and the Suez Canal (Table S1) negatively. This factor could, therefore, be interpreted as an indicator of the salinity level of the waters resulting from the equilibrium of lateral fresh and saltwater supplies. On the second long-range factor with an eigenvalue greater than 1, which explained 21.18% of the spatial variance at this scale, calcium, potassium, and distance from the Suez Canal primarily contribute positively, whereas total depth and distance from the Damietta branch contribute negatively. This factor could, therefore, be interpreted as an indicator of water quality, particularly for calcium and potassium content. On the third long-range factor with an eigenvalue greater than 1, which explained only 14.5% of the spatial variance at this scale, the distances from the Damietta branch and Lake Manzala, bicarbonate, and water level weigh negatively. Indeed, giving a physical interpretation to this factor is rather difficult, showing an inverse relationship between water table depth and bicarbonate content. The fourth long-range factor with an eigenvalue greater than 1 explained a variance rate of less than 10%, so it was decided to neglect it. In the short range, there were no factors with eigenvalues greater than 1.

In 2007 (Table S5), the first short-range factor with an explained variance of 35.87% was positively correlated with Ca and Mg and, to a lesser extent, with Cl and EC and negatively correlated with pH. It could then be interpreted as an indicator of the level of solutes in the waters. The retained second short-range factor, with an explained variance percentage of 28.55, was negatively correlated with Cl, EC, Na, pH, and total depth. It could then be assumed as an inverse indicator of the salinization level and then of the water quality.

In the same survey, there were two regionalized long-range factors with eigenvalues greater than one. The first factor explained 64.7% of the variance at this scale and was positively correlated with Cl and Na and negatively correlated with distance from Lake Manzala and water level. It could then be assumed to be an indicator of saline water intrusion from Lake Manzala. The second factor, which explained only about 28% of the spatial variance, was positively correlated with distance from the Suez Canal (saltwater) and negatively correlated with distance from the Damietta branch (freshwater). Therefore, this factor could also be interpreted as an indicator of the salinization level of the waters (an inverse indicator of water quality) resulting from the balance of saline and freshwater supply.

Finally, in the 2018 survey (Table S6), the first long-range factor, which explained 71.9% of the scale variance, was mostly positively correlated with Cl, EC, Na, Mg, and SO_4 and negatively correlated with distance from Lake Manzala. It is then a clear indicator of the salinity of the waters resulting from the proximity of the salty lake. The second factor explained 20.55% of the scale variance and was positively correlated with distance from the Suez Canal and negatively correlated with bicarbonate content, which could be taken as an inverse indicator. The third factor explained less than 10% of the scale variance and was then omitted. In the short range, there were no factors with eigenvalues greater than 1.

Mapping the first factors in the three surveys

It was, therefore, decided to take the first long-range factor for the three surveys as a scale-consistent indicator of the level of salinization of the waters. A partition of the study area into three macro-areas of equal size, each comprising approximately 33% of the total number of pixels, was made for each survey. Although the level of salinization and its gradient change in the three surveys (the three color scales are not the same), as it is evident also from the previous investigations, there was a consistent downward trend in salinity in the NE/SW direction during the whole period 1996–2018 of study. This decrease is manifested in a compact southwestern area and in a more irregular central-eastern area with alternations of zones with different salinity (Figure 10).

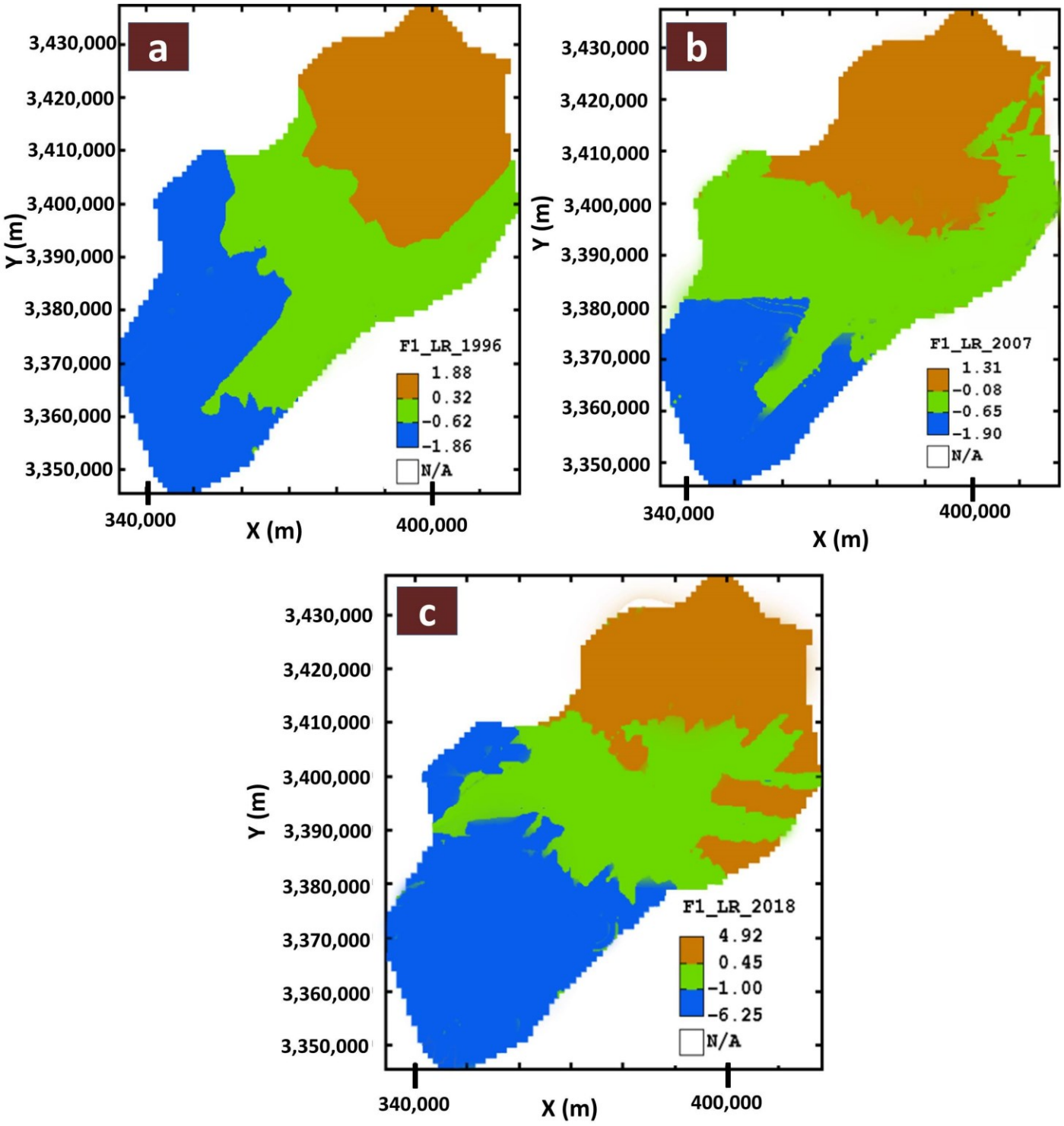

Figure 10. First Factor (LMC at long range): (**a**) 1996; (**b**) 2007; (**c**) 2018.

4. Discussion

The chemical classification of groundwater represented in the Schoeller Berkaloff diagrams (Figure S1) generally shows an increase of sodium chloride over time and a related increase in total salinity (graphs C, F, and I in Figure S1). Furthermore, they show a decrease in calcium bicarbonate over time (graphs B, E, and H in Figure S1). The comparative analysis with the spatial distribution (Figures 3–7) and with the variation over time of the main chemical parameters represented in the Q-Q plots (Figures 8 and 9) allows us to affirm that the increase in sodium chloride water occurred due to migration towards the southwest at the expense of volumes of calcium bicarbonate water. The comparative analysis with the reconstruction of the piezometric surface over time (Figure 3) also allows us to ascribe the aforementioned variations to a general decrease in the water level, starting from a situation of equilibrium in 1996 up to a situation of general pumping with the presence of localized pumping areas capable of drawing brackish water from Lake Manzala.

In general, it is possible to note that over 22 years, there has been an increase in sodium chloride, a general increase in the total salinity of the waters, and a migration of water salinization towards the southwest.

Compared to this general trend, the central band, approximately 35 km wide and extending approximately 10–20 km north of the Ismailia Canal, presents piezometric and chemical structures between 2007 and 2018 that are peculiar and different from the general structure described above. The piezometric surface from 2007 to 2018 evolves into a lobed shape, which highlights the alternation of piezometric highs and lows, which testify to the decrease, albeit not homogeneous, in pumping. In this area, we also observe the following:

- in 2018, the appearance of two zones of groundwater salinity less than 2 dS/m (Figure 4);
- a decrease in the concentration of Cl and Na (Figures 5 and 6);
- an increase in Ca concentration in 2018 (Figure 7).

The Ca concentration shows an inverse trend compared to that of Na and Cl. In 2007, the Ca concentration decreased compared to that of 1996 because the sodium chloride waters replaced the bicarbonate ones with an increase in salinity due to the decrease in the hydraulic load, which draws salt/brackish water from Manzala Lake. In 2018, at the same time as the uneven decrease in pumping, a recovery in the concentration of Ca and a slight decrease in Cl and Na were observed, probably due to the recall of bicarbonate surface water (i.e., not sodium chloride) from the Ismailia channel. The piezometric surface reconstructed in 2018, in fact, shows a water flow from the Ismailia canal towards the northern area.

The analysis of the raw chemical data and their spatial distribution estimated in three-time windows show, therefore, a generalized decrease in the water level with a consequent increase in salinity and Na and Cl content over time and towards the southwest. This trend appears to be mitigated in the central part of the study area, where the decrease in pumping rates (even if not in a homogeneous way) and the recall of surface water from the Ismailia Canal attenuate salinization and generate an increase in Ca content.

The above-described geospatial and multi-temporal distribution of ion concentration, salinity, and water level (piezometric surface) was implemented with the identification of homogeneous zones based on the kriging factorial analysis that considered the distance from the salty (Suez Canal and Manzala Lake) and fresh (Damietta Branch and Ismailia Canal) surface water bodies as auxiliary variables. The result of such analysis clearly highlights the influence of the above-mentioned surface water bodies in the evolution of the chemistry of the groundwater both over time and space. In fact, a general increase in water salinity from the northeast to the southwest was shown (Figure 10) due to the lowering of the water level (Figure 3) and the consequent recall of water from

Manzala Lake in the period from 1998 to 2007. Differently, a decrease in salinity in 2018 (Figure 10) was estimated due to probable decreases in pumping rates, which caused a slight decrease in salinity in the southwestern part and an irregular decrease in salinity, Cl, and Na concentration in the central-eastern part (Figures 4–6 referred to 2018). This was probably due to the decrease in pumping rates and the recall of freshwater from Ismailia Chanel, as highlighted by the distribution of water levels (Figure 3).

As demonstrated in Figure 5, the northern region of the study area exhibits symptoms of SWI, characterized by an average water salinity level of 6–8 dS/m in 1996. However, a comparatively smaller area in the northernmost region demonstrates levels exceeding 10 dS/m. Furthermore, in 2007 and 2018, the area affected by water salinity levels greater than 10 dS/m expanded, indicating a significant escalation in this phenomenon. This rise in water salinity, particularly from 6 dS/m, is anticipated to have a deleterious effect on soil and crop yield in the regions where these levels are present. The study area is predominantly cultivated with field crops, including wheat, barley, maize, rice, sorghum, tomato, lettuce, cabbage, cucumber, and beans. The continued increase in groundwater salinity is anticipated to have a deleterious effect on the yield of these crops, particularly those of wheat, rice, and maize, which are considered to be of strategic importance. It is important to note that the ongoing utilization of groundwater for irrigation in the northern region, particularly in areas where salinity levels exceed 10 dS/m, may result in a significant reduction in crop yield, ranging from 20% to 100%, for the aforementioned crops. Additionally, the ongoing use of high-salinity groundwater for irrigation purposes is likely to have a detrimental effect on the stability of soil aggregates. The results obtained in this study largely align with previous studies in the area, which indicated that there is a prolonged increase in groundwater salinity due to continuous over-pumping from the Nile Delta aquifer for different purposes [7,32,43,62].

5. Conclusions

The proposed multidisciplinary approach, based on the chemical analysis of raw data and their spatial interpolation using multivariate geostatistical techniques, allowed the evaluation of the temporal evolution and the extent of saltwater intrusion in the eastern portion of the Nile Delta.

In particular, the dependence of the groundwater chemical parameters on the distance between salt and fresh surface water bodies was introduced for the first time. The distances to salt and freshwater bodies in the Linear Model of Coregionalization, as auxiliary variables, made the spatial distribution of key variables obtained by Ordinary Cokriging more reliable and physically based.

Factorial Kriging analysis using Gaussian estimates of Ordinary Cokriging provided the multi-temporal distribution of the aquifer salinization process.

Among the limitations of the analysis carried out, which have conferred uncertainty in the evaluation of the space-time variability, it is worth highlighting the chemical low-frequency monitoring campaigns that have not allowed a continuous recording of the phenomenon and the non-coincidence of the monitoring locations in the three survey campaigns.

A more accurate analysis with more robust results would make it possible to define an optimal uniformly distributed network of survey points, coupled with regular and more frequent monitoring of groundwater even along the vertical dimension. Hopefully, continuous monitoring of salinity at least should be foreseen. Equal importance would be the monitoring of the flow rate and chemical-physical characteristics of the Nile canals, which can interact with the groundwater both naturally and through irrigation.

Such a monitoring network would allow for physically-based management of groundwater and surface water resources with the possibility of modulating demand with

availability, considering the risk of salinization but also the possibility of blunting the salinization phenomenon through irrigation with fresh water from canals. The availability of data in space and time would enable the use of density-dependent mathematical modeling aimed at rational and efficient deep and surface water management.

Supplementary Materials: The following supporting information can be downloaded at www.mdpi.com/xxx/s1, Figure S1. Schoeller Berkaloff Diagram. A, D, and G: all samples analyzed in 1996, 2007, and 2018, respectively. B, E, and H: only samples with predominantly calcium or sodium bicarbonate chemistry in 1996, 2007, and 2018, respectively; C, F, and I: sodium chloride chemistry samples in 1996, 2007, and 2018, respectively. Table S1. Linear model of coregionalization of the transformed Gaussian variables in 1996. The coregionalization matrices are reported (sills of variograms). Table S2. Linear model of coregionalization of the transformed Gaussian variables in 2007. The coregionalization matrices are reported (sills of variograms). Table S3. Linear model of coregionalization of the transformed Gaussian variables in 2018. The coregionalization matrices are reported (sills of variograms). Table S4. Structure of the regionalized factors whose eigenvalue is greater than 1 by spatial scale in 1996. Table S5. Structure of the regionalized factors whose eigenvalue is greater than 1 by spatial scale in 2007. Table S6. Structure of the regionalized factors whose eigenvalue is greater than 1 by spatial scale in 2018.

Author Contributions: Conceptualization, S.S., A.C., D.D.C., S.R., H.S.A.S. and A.M.N.; methodology, S.S., A.C., D.D.C., S.R., H.S.A.S. and A.M.N.; software, S.S., A.C., D.D.C., S.R., H.S.A.S. and A.M.N.; validation, S.S., A.C., D.D.C., S.R., H.S.A.S. and A.M.N.; formal analysis, S.S., A.C., D.D.C., S.R., H.S.A.S. and A.M.N.; investigation, S.S., A.C., D.D.C., S.R. H.S.A.S., and A.M.N.; resources, S.S., A.C., D.D.C., S.R., H.S.A.S. and A.M.N.; data curation, S.S., A.C., D.D.C., S.R., H.S.A.S. and A.M.N.; writing—original draft preparation, S.S., A.C., D.D.C., S.R., H.S.A.S. and A.M.N.; writing—review and editing, S.S., A.C., D.D.C., S.R., H.S.A.S. and A.M.N.; visualization, S.S., A.C., D.D.C., S.R., H.S.A.S. and A.M.N. All authors have read and agreed to the published version of the manuscript.

Funding: This research received no external funding.

Data Availability Statement: Data are contained within the article and Supplementary Materials.

Acknowledgments: The authors would like to thank the Environmental Geophysics Lab (ZEGL), Geology Department, Faculty of Science, Zagazig University, for supporting the fieldwork (sampling process "year 2018").

Conflicts of Interest: The authors declare no conflicts of interest.

References

1. Hugo, G. Future demographic change and its interactions with migration and climate change. *Glob. Environ. Change* **2011**, *21*, S21–S33.
2. Shi, L.; Jiao, J.J. Seawater intrusion and coastal aquifer management in China: A review. *Environ. Earth Sci.* **2014**, *72*, 2811–2819.
3. Hounsinou, S.P. Assessment of potential seawater intrusion in a coastal aquifer system at Abomey-Calavi, Benin. *Heliyon* **2020,** *6*, e03173.
4. Jasechko, S.; Perrone, D.; Seybold, H.; Fan, Y.; Kirchner, J.W. Groundwater level observations in 250,000 coastal US wells reveal scope of potential seawater intrusion. *Nat. Commun.* **2020**, *11*, 3229.
5. El Shinawi, A.; Zeleňáková, M.; Nosair, A.M.; Abd-Elaty, I. Geo-spatial mapping and simulation of the sea level rise influence on groundwater head and upward land subsidence at the Rosetta coastal zone, Nile Delta, Egypt. *J. King Saud Univ.-Sci.* **2022**, *34*, 102145.
6. Werner, A.D.; Bakker, M.; Post, V.E.; Vandenbohede, A.; Lu, C.; Ataie-Ashtiani, B.; Simmons, C.T.; Barry, D.A. Seawater intrusion processes, investigation and management: Recent advances and future challenges. *Adv. Water Resour.* **2013**, *51*, 3–26.
7. Abu Salem, H.S.; Gemail, K.S.; Junakova, N.; Ibrahim, A.; Nosair, A.M. An integrated approach for deciphering hydrogeochemical processes during seawater intrusion in coastal aquifers. *Water* **2022**, *14*, 1165.

8. Robinson, G.; Hamill, G.; Ahmed, A.A. Automated image analysis for experimental investigations of salt water intrusion in coastal aquifers. *J. Hydrol.* **2015**, *530*, 350–360.
9. Sefelnasr, A.; Sherif, M. Impacts of seawater rise on seawater intrusion in the Nile Delta aquifer, Egypt. *Groundwater* **2014**, *52*, 264–276.
10. Lu, C.; Xin, P.; Li, L.; Luo, J. Seawater intrusion in response to sea-level rise in a coastal aquifer with a general-head inland boundary. *J. Hydrol.* **2015**, *522*, 135–140.
11. Abdoulhalik, A.; Ahmed, A.A. The effectiveness of cutoff walls to control saltwater intrusion in multi-layered coastal aquifers: Experimental and numerical study. *J. Environ. Manag.* **2017**, *199*, 62–73.
12. Pulido-Velazquez, D.; Renau-Pruñonosa, A.; Llopis-Albert, C.; Morell, I.; Collados-Lara, A.-J.; Senent-Aparicio, J.; Baena-Ruiz, L. Integrated assessment of future potential global change scenarios and their hydrological impacts in coastal aquifers—A new tool to analyse management alternatives in the Plana Oropesa-Torreblanca aquifer. *Hydrol. Earth Syst. Sci.* **2018**, *22*, 3053–3074.
13. Nlend, B.; Celle-Jeanton, H.; Huneau, F.; Ketchemen-Tandia, B.; Fantong, W.; Boum-Nkot, S.N.; Etame, J. The impact of urban development on aquifers in large coastal cities of West Africa: Present status and future challenges. *Land Use Policy* **2018**, *75*, 352–363.
14. Abija, F.; Abam, T.; Teme, S.; Eze, C. Relative sea level rise, coastline variability and coastal erosion in the Niger Delta, Nigeria: Implications for climate change adaptation and coastal zone management. *Earth Sci. Clim. Change* **2020**, *11*, 9.
15. Prusty, P.; Farooq, S.H. Seawater intrusion in the coastal aquifers of India-A review. *HydroResearch* **2020**, *3*, 61–74.
16. Arslan, H.; Demir, Y. Impacts of seawater intrusion on soil salinity and alkalinity in Bafra Plain, Turkey. *Environ. Monit. Assess.* **2013**, *185*, 1027–1040.
17. Qu, W.; Li, H.; Huang, H.; Zheng, C.; Wang, C.; Wang, X.; Zhang, Y. Seawater-groundwater exchange and nutrients carried by submarine groundwater discharge in different types of wetlands at Jiaozhou Bay, China. *J. Hydrol.* **2017**, *555*, 185–197.
18. Boumaiza, L.; Walter, J.; Chesnaux, R.; Zahi, F.; Huneau, F.; Garel, É.; Stotler, R.L.; Bordeleau, G.; Johannesson, K.H.; Vystavna, Y. Combined effects of seawater intrusion and nitrate contamination on groundwater in coastal agricultural areas: A case from the Plain of the El-Nil River (North-Eastern Algeria). *Sci. Total Environ.* **2022**, *851*, 158153.
19. Ferguson, G.; Gleeson, T. Vulnerability of coastal aquifers to groundwater use and climate change. *Nat. Clim. Change* **2012**, *2*, 342–345.
20. Vespasiano, G.; Cianflone, G.; Romanazzi, A.; Apollaro, C.; Dominici, R.; Polemio, M.; De Rosa, R. A multidisciplinary approach for sustainable management of a complex coastal plain: The case of Sibari Plain (Southern Italy). *Mar. Pet. Geol.* **2019**, *109*, 740–759.
21. Elewa, H.H.; Nosair, A.M.; Zelenakova, M.; Mikita, V.; Abdel Moneam, N.A.; Ramadan, E.M. Environmental sustainability of water resources in coastal aquifers, case study: El-Qaa Plain, South Sinai, Egypt. *Water* **2023**, *15*, 1118.
22. Kouzana, L.; Mammou, A.B.; Felfoul, M.S. Seawater intrusion and associated processes: Case of the Korba aquifer (Cap-Bon, Tunisia). *Comptes Rendus. Géoscience* **2009**, *341*, 21–35.
23. Gemail, K.; Samir, A.; Oelsner, C.; Mousa, S.; Ibrahim, S. Study of saltwater intrusion using 1D, 2D and 3D resistivity surveys in the coastal depressions at the eastern part of Matruh area, Egypt. *Near Surf. Geophys.* **2004**, *2*, 103–109.
24. Agoubi, B. A review: Saltwater intrusion in North Africa's coastal areas—Current state and future challenges. *Environ. Sci. Pollut. Res.* **2021**, *28*, 17029–17043.
25. Carreira, P.M.; Bahir, M.; Salah, O.; Fernandes, P.G.; Nunes, D. Tracing salinization processes in coastal aquifers using an isotopic and geochemical approach: Comparative studies in western Morocco and southwest Portugal. *Hydrogeol. J.* **2018**, *26*, 2595–2615.
26. Campillo, A.; Taupin, J.-D.; Betancur, T.; Patris, N.; Vergnaud, V.; Paredes, V.; Villegas, P. A multi-tracer approach for understanding the functioning of heterogeneous phreatic coastal aquifers in humid tropical zones. *Hydrol. Sci. J.* **2021**, *66*, 600–621.
27. Xiao, H.; Wang, D.; Medeiros, S.C.; Hagen, S.C.; Hall, C.R. Assessing sea-level rise impact on saltwater intrusion into the root zone of a geo-typical area in coastal east-central Florida. *Sci. Total Environ.* **2018**, *630*, 211–221.
28. Mastrocicco, M.; Busico, G.; Colombani, N.; Vigliotti, M.; Ruberti, D. Modelling actual and future seawater intrusion in the Variconi coastal wetland (Italy) due to climate and landscape changes. *Water* **2019**, *11*, 1502.
29. Younes, A.; Koohbor, B.; Belfort, B.; Ackerer, P.; Doummar, J.; Fahs, M. Modeling variable-density flow in saturated-unsaturated porous media: An advanced numerical model. *Adv. Water Resour.* **2022**, *159*, 104077.
30. Xiong, G.; Chen, G.; Wu, J.; Fu, T.; Yang, Y.; Xu, X.; Zhu, X.; Yu, H.; Liu, S.; Gao, M. Seawater intrusion-retreat processes and groundwater evolution in intruded coastal aquifers with land reclamation: A case study of Eastern Jiangsu, China. *Lithosphere* **2022,** 1308487.

31. Lal, A.; Datta, B. Development and implementation of support vector machine regression surrogate models for predicting groundwater pumping-induced saltwater intrusion into coastal aquifers. *Water Resour. Manag.* **2018**, *32*, 2405–2419.
32. Nosair, A.M.; Shams, M.Y.; AbouElmagd, L.M.; Hassanein, A.E.; Fryar, A.E.; Abu Salem, H.S. Predictive model for progressive salinization in a coastal aquifer using artificial intelligence and hydrogeochemical techniques: A case study of the Nile Delta aquifer, Egypt. *Environ. Sci. Pollut. Res.* **2022**, *29*, 9318–9340.
33. Panagiotou, C.F.; Kyriakidis, P.; Tziritis, E. Application of geostatistical methods to groundwater salinization problems: A review. *J. Hydrol.* **2022**, *615*, 128566.
34. Tizro, A.T.; Fryar, A.E.; Voudouris, K.; Talebi, M. Prediction of water-level variations using a combined time series-geostatistical model in an aquifer surrounded by karstic formation: A case study from the semi-arid Hamadan province, Iran. *preprint* 2023.
35. Zhou, S.; Gao, Y.; Zhang, J.; Pang, J.; Hamani, A.K.M.; Xu, C.; Dang, H.; Cao, C.; Wang, G.; Sun, J. Impacts of Saline Water Irrigation on Soil Respiration from Cotton Fields in the North China Plain. *Agronomy* **2023**, *13*, 1197. https://doi.org/10.3390/agronomy13051197.
36. Ayers, R.S.; Westcot, D.W. *Water Quality for Agriculture*; FAO Irrigation and Drainage, Paper 29; Food and Agriculture Organization: Rome, Italy1985.
37. Sherif, M.; Sefelnasr, A.; Javadi, A. Incorporating the concept of equivalent freshwater head in successive horizontal simulations of seawater intrusion in the Nile Delta aquifer, Egypt. *J. Hydrol.* **2012**, *464*, 186–198.
38. Mazi, K.; Koussis, A.D.; Destouni, G. Intensively exploited Mediterranean aquifers: Resilience to seawater intrusion and proximity to critical thresholds. *Hydrol. Earth Syst. Sci.* **2014**, *18*, 1663–1677.
39. Webster, R.; Oliver, M.A. *Geostatistics for Environmental Scientists*; John Wiley & Sons: Hoboken, NJ, USA, 2007.
40. Castrignanò, A.; Buttafuoco, G.; Conforti, M.; Maesano, M.; Moresi, F.V.; Mugnozza, G.S. Improving the Spatial Prediction of Sand Content in Forest Soils Using a Multivariate Geostatistical Analysis of LiDAR and Hyperspectral Data. *Remote Sens.* **2023**, *15*, 4416.
41. Mohammed, M.S.; Elbeih, S.F.; Mohamed, E.A.; Abu Salem, H.S.; Ibrahim, M.; ElSayed, E.E. Spectral indices based study to evaluate and model surface water quality of Beni Suef Governorate. Egypt. *Egypt. J. Chem.* **2022**, 65, 631–645.
42. El-Marsafawy, S.; Bakr, N.; El-Bana, T.; El-Ramady, H. Climate. In *The Soils of Egypt*; World Soils Book Series; El-Ramady, H., Alshaal, T., Bakr, N., Elbana, T., Mohamed, E., Belal, A.-A., Eds.; Springer: Cham, Switzerland, 2019. https://doi.org/10.1007/978-3-319-95516-2_3.
43. Elewa, H.H.; Shohaib, R.E.; Qaddah, A.A.; Nousir, A.M. Determining groundwater protection zones for the Quaternary aquifer of northeastern Nile Delta using GIS-based vulnerability mapping. *Environ. Earth Sci.* **2013**, *68*, 313–331.
44. Sallouma, M.K.M. Hydrogeological and Hydrochemical Assessment of the Quaternary Aquifer in the Eastern Nile Delta, Egypt. Ph.D. Thesis, Ain Shams University, Cairo, Egypt, 1983.
45. Said, R. *The Geological Evolution of the River Nile*; Springer: Berlin/Heidelberg, Germany; New York, NY, USA, 1981; 151p.
46. Ismael, A.M.A.A. *Applications of Remote Sensing, GIS, and Groundwater Flow Modeling in Evaluating Groundwater Resources: Two Case Studies; East Nile Delta, Egypt and Gold Valley, California, USA*; The University of Texas at El Paso: El Paso, TX, USA, 2007.
47. Ramadan, E.M.; Fahmy, M.R.; Nosair, A.M.; Badr, A.M. Using geographic information system (GIS) modeling in evaluation of canals water quality in Sharkia Governorate, East Nile Delta, Egypt. *Model. Earth Syst. Environ.* **2019**, *5*, 1925–1939.
48. Tantawi, M. Hydrogeochemical and isotopic assessment of the Quaternary aquifer in the Eastern Nile Delta, Egypt. *El-Minia Sci. Bull.* **1998**, *11*, 17–45.
49. Rizk, T. Hydrogeological Studies on El Salhyia District, East Nile Delta, Egypt. Master's Thesis, Mansoura University, Mansoura, Egypt, 1997.
50. Di Curzio, D.; Castrignanò, A.; Fountas, S.; Romić, M.; Rossel, R.A.V. Multi-source data fusion of big spatial-temporal data in soil, geo-engineering and environmental studies. *Sci. Total. Environ.* **2021**, *788*, 147842.
51. Chiles, J.-P.; Delfiner, P. *Geostatistics: Modeling Spatial Uncertainty*; John Wiley & Sons: New York, NY, USA, 2012; Volume 713.
52. Wackernagel, H. *Multivariate Geostatistics: An Introduction with Applications*; Springer Science & Business Media: Berlin/Heidelberg, Germany, 2003.
53. Howarth, R. Journel and (Ch. J.) Huijbregts. Mining Geostatistics. London & New York (Academic Press), 1978. x+ 600 pp. 267 figs. Price£ 32· 00. *Mineral. Mag.* **1979**, *43*, 563–564.
54. Goovaerts, P. *Geostatistics for Natural Resources Evaluation*; Oxford University Press: Oxford, UK, 1997; Volume 483.
55. Rivoirard, J. Which models for collocated cokriging? *Math. Geol.* **2001**, *33*, 117–131.
56. Castrignanò, A. *Introduction to Spatial Data Analysis*; Aracne, Rome: Rome, Italy, 2011.
57. Cressie, N.A.C. *Statistics for Spatial Data;* John Wiley and Sons Inc.: Hoboken, NJ, USA, 1993.

58. Abu Salem, H.S.; El Fallah, O.A.; El Kammar, M.M. Hydrochemical study of groundwater in Tazerbo, Libya, using statistical analysis and geochemical modeling. *J. Afr. Earth Sci*. **2024**, *218*, 105362.
59. Hussein, H.; El Maghraby, M.M.; Abu Salem, H.S. Application of water quality index and statistical-hydrochemical techniques in groundwater assessment of the Quaternary aquifer, southwest Nile Delta of Egypt. *Appl. Water Sci.* **2024**, *14*(6), 143.
60. Castrignanò, A.; Giugliarini, L.; Risaliti, R.; Martinelli, N. Study of spatial relationships among some soil physico-chemical properties of a field in central Italy using multivariate geostatistics. *Geoderma* **2000**, *97*, 39–60.
61. Appelo, C.A.J.; Postma, D. *Geochemistry, Groundwater and Pollution*; CRC Press: Balkema, Roterdam , 2004.
62. Arafa, N.A.; Salem, Z.El.; Abdeldayem, A.L.; Ghorab, M.A.; Moustafa, Y.M.; Soliman, S.A.; Purohit, S.; Elhag, M.; Youssef, Y.M. Advancing Deltaic Aquifer Vulnerability Mapping to Seawater Intrusion and Human Impacts in Eastern Nile Delta: Insights from Machine Learning and Hydrochemical Perspective. *Earth Syst. Environ.* **2024**, 1–26. https://doi.org/10.1007/s41748-024-00518-6.